Seasonal water storage in peat-forming bofedales sustains baseflow in the Andes

Wyeth Wunderlich[1], Margaret Lang[2], Kristina Keating[3], Wilner Bandera Perez[4],

Jasper Oshun [5]

1 *California Polytechnic University, Humboldt, Department of Geology.*

2 *California Polytechnic University, Humboldt, Department of Environmental Resources Engineering.*

3 *Rutgers University Newark, Department of Earth and Environmental Sciences*

4 *Universidad Nacional de San Antonio Abad del Cusco (UNSAAC), Departamento de Geología.*

5 U.S. Fulbright Scholar and Visiting Professor at the Universidad de Ingeniería y Tecnología, Lima, Perú

Seasonal water storage in peat-forming bofedales sustains baseflow in the Andes

Wyeth Wunderlich[1], Margaret Lang[2], Kristina Keating[3], Wilner Bandera Perez[4],

Jasper Oshun [5]

1 *California Polytechnic University, Humboldt, Department of Geology.*

2 *California Polytechnic University, Humboldt, Department of Environmental Resources Engineering.*

3 *Rutgers University Newark, D.*

4 *Universidad Nacional de San Antonio Abad del Cusco (UNSAAC), Departamento de Geología.*

5 *U.S. Fulbright Scholar and Visiting Professor at the Universidad de Ingeniería y Tecnología, Lima, Perú*

Abstract

Region: Humid puna of the Central Andes

Focus: Bofedales, or low gradient peat-forming wetlands, are a characteristic feature of the humid puna - a high elevation, seasonally dry grass- and shrub-land found throughout the Central Andes. Despite the importance of the humid puna in supplying water to downstream communities, and the inference that bofedales may play an important role, few studies have explored the hydrology of the humid puna, and none have quantified the amount of water bofedales contribute to streamflow. We designed a 3-year study in the Upper Ramuschaka Watershed (URW), a 2.12 km^2 humid puna catchment sustaining a perennial stream used for irrigation. We monitored precipitation, subsurface moisture, bofedal groundwater, and streamflow, measured discharge in 19 nested subbasins through the wet and dry seasons, and investigated the structure and hydraulic properties of bofedales.

Hydrological Insights: We discovered a positive relationship between unit runoff and the percent of bofedal cover across subbasins. Bofedales collect groundwater from areas 4-12 times their size, store large volumes in high porosity peat, and release water to streams through lower conductivity layers. Bofedales cover 11.6% of the URW, dynamically store 105,000 m^3 ± 10,000 of water and yield 49 ± 5 mm to streams in the dry season, accounting for 20 – 98% of catchment-wide dry season runoff. Bofedales regulate drainage from the humid puna to downstream communities and are therefore vital to local and regional water security.

Keywords: bofedales; puna; water resources; wetlands; natural infrastructure; nuclear magnetic resonance

1.0 Introduction

The humid puna, a seasonally dry alpine grass- and shrub-land that exists at the altitudinal limits of plant survival, sustains perennial streams identified as important water sources throughout the Central Andes (Squeo et al., 2006; Bradley et al., 2006; Vuille et al., 2008; Buytaert et al., 2009, Celleri et al., 2010; Maldanado Fonken, 2014; Drenkhan et al., 2015; Ochoa-Tocachi et al., 2016). The humid puna is found between 8° S and 15° S latitude, at elevations between 2,000 and 6,000 m.a.s.l. and currently covers an estimated 18.6% (236,220 km^2) of the Tropical Andes from central Perú through northeastern Bolivia (e.g., Josse et al., 2009). Under the Intergovernmental Panel on Climate Change (IPCC) carbon emissions scenario A1B (1° C to 1.5° C projected regional temperature increase) an estimated 21.6% of glacierized and cryoturbated land area in the Tropical Andes will be replaced by humid puna from 2010 to 2039 (Tovar et al., 2013). As the climate warms and the humid puna migrates upslope, understanding and predicting changes to local and regional hydrologic processes will be vital to future water security.

Mean annual precipitation in the humid puna varies from 600 mm to 2,000 mm, resulting in a wetter climate than the dry puna found in Argentina and Chile and a drier climate than the jàlca and páramo biomes of the northern Andes (Squeo et al., 2006; Josse et al., 2009; Tovar et al., 2013; Ochoa-Tocachi et al., 2016). Precipitation in the humid puna falls primarily between December and April, with a near-absence of precipitation from May to August (e.g., Squeo et al., 2006; Garreaud, 2009; Drenkhan et al., 2015; Ochoa-Tocachi et al., 2016; Aybar et al., 2020). Stream discharge contains significant contributions from precipitation-fed groundwater, even in watersheds receiving glacial meltwater (e.g., Baraer et al., 2009; Somers et al., 2009; Buytaert et al, 2017; Glas et al., 2019; Somers et al., 2019), which suggests large and seasonally dynamic water storage within the puna landscape.

The landscape of the puna is characterized by complex topography of steep hillslopes, prominent ridges, and exposed bedrock outcrops (Josse et al., 2009; Oliveras et al., 2014; Ochoa-Tocachi et al., 2016). The landscape often shows glacial features, such as steep, amphitheater shaped uplands of exposed bedrock or tussock grasses draining to low gradient basins filled with quaternary fluvial, glaciofluvial, and/or colluvial deposits (Josse et al., 2009; Somers and McKenzie, 2020). These basins host wetlands known as 'bofedales' (singular: 'bofedal') - seasonally or perennially saturated peat-forming alpine wetlands with distinct hydrophytic plant assemblages found in topographic depressions, valley bottoms and along watercourses within the humid and dry puna (Cooper et al., 2009; Squeo et al., 2006; Josse et al., 2009; Maldanado Fonken, 2014; Salvador et al., 2014; Polk et al. 2019). The extent of bofedales in the Pervuian Andes is estimated to be nearly 550 km^2 (Ministry of the Environment, Perú, 2019). Bofedales are important 'cultural landscapes' (e.g., White-Nockelby et al.,, 2021) that have long provided grazing grounds for Andean camelids (e.g., Palacios Ríos, 1977; Orlove, 1977; Bryant and Farfan, 1984; Reiner and Bryant, 1986; Patty et al., 2010), have been linked to the presence and expansion of human settlements (e.g., Vining et al., 2019), and have been managed and expanded to sustain local water resources (Flores-Ochoa, 1977; Palacios Ríos, 1977; Erickson, 2000; Lane, 2006, 2009, and 2013, 2014; Vining et al., 2019; Uribe-Álvarez et al., 2021).

Bofedales are inferred to be a 'natural' or 'green' infrastructure (e.g., Argüello 2018 ; Castillo and Crisman, 2019; López Gonzales et al., 2020) believed to seasonally capture, store, and release water; therein providing source water buffered from the seasonality of rainfall (e.g., Earle et al., 2003; Flores et al., 2014; Maldanado Fonken et al., 2014; Salvador et al., 2014; Drenkhan et al., 2015). Here, we introduce the words 'natural' and 'green' while acknowledging many bofedales are 'socio-hydrological' systems (Yager et al., 2021) with a long history of indigenous management (as cited in the previous paragraph). Two factors likely contribute to the inference that bofedales represent a natural infrastructure. First, bofedales contain layers of high porosity peat that can be up to 10 m thick (Hribljan et al., 2015; Engel et al., 2014; Cooper et al., 2019), which can store large quantities of water (e.g., Cooper, 2019; Valois et al., 2020; Valois et al., 2021). Secondly, as post-glacial features, bofedales are often found in lower gradient basins fed by large contributions of upslope groundwater (e.g., Gordon et al., 2015; Cooper et al., 2019). Although they are peat forming, bofedales are minerotrophic fens fed by groundwater rather than ombrotrophic bogs (Squeo 2006; Cooper et al. 2010, 2019; Maldonado Fonken 2014; Salvador et al. 2014; Hribljan et al. 2016; Oyague et al., 2022). Whereas geophysical and hydrochemical methods have been used to estimate porosity and total water storage in bofedales (e.g., Valois et al., 2020; Valois et al., 2021), no study has yet quantified seasonally dynamic water storage in bofedales and linked these results to seasonal patterns in catchment water yield.

Our study is focused on the Upper Ramuschaka Watershed (URW), a 2.12 km^2 headwater catchment in the humid puna with 11.6% of its area (24.6 ha) covered in bofedales. The URW is located within the Vilcanota–Urubamba Basin (VUB), a northwest flowing river system encompassing an area of 11,048 km^2 (Drenkhan et al., 2018). Approximately 1,000,000 people live in the VUB, and most depend on water resources draining the humid puna (SEDACUSCO EPS, 2019). Approximately 78.2% of the VUB is covered in puna (Oshun et al., 2021; Josse et al., 2009; Ochoa-Tocachi et al., 2016) and the VUB hydrograph follows seasonal precipitation patterns – peaking during the wet season (December to April) and declining slowly through the dry season (Drenkhan et al., 2015, EGESMA, Oshun et al., 2021). Glacier meltwater accounts for less than 2% of annual runoff in the VUB at larger watershed scales (Buytaert et al., 2017), with the vast majority of annual runoff coming from groundwater, and baseflow from the puna sustaining dry season flows (Fernandez-Palomino et al., 2021).

The URW provides water to the agrarian district of Zurite (pop. 3,640; *Municipalidad Distrital de Zurite*, 2017), located at an elevation of 3,405 m.a.s.l. in the province of Anta, 40 km northwest of Cusco. Mean annual precipitation in Zurite (1981 – 2017) is 848 mm, 95% of which typically falls between October and April, with the remaining 5% between May and September (Aybar et al., 2020). The community of Zurite relies entirely on humid puna-derived water resources for agricultural and municipal use, much of which drains from the URW. Water is sourced primarily from the diversion and distribution through traditional surface water canals is managed by a local water commission (Oshun et al., 2021). Although there are 4 small reservoirs, the combined storage capacity is approximately equivalent to one day's irrigation demand in the dry season. Dependence on local water resources, a pronounced dry season, and a lack of long-term water storage results in vulnerability to the approximately 5-month seasonal drought as well as, longer-term climatically driven changes in water resources.

The URW thus represents a model watershed to explore the role of bofedales in sustaining societally important water resources in the humid puna. Specifically, we asked the following:

1) What are the annual and seasonal water yields from the URW, a humid puna watershed?
2) What are the temporal patterns linking precipitation to unsaturated zone storage inside hillslopes, groundwater storage in bofedales and runoff generation in the URW?

3) What are the spatiotemporal patterns of runoff across the varied landscape of the URW?
4) What is the quantity of seasonally dynamic water storage in bofedales and what proportion of dry season runoff comes from bofedal drainage?

To answer these questions, we collected hydrogeologic data over three water years (WY): WY2019 (1 September 2018 to 31 August 2019), WY2020 (1 September 2019 to 31 August 2020), and WY2021 (1 September 2020 to 31 August 2021). We employed an integrated local environmental knowledge approach, which incorporated traditional and western scientific approaches to knowledge production and is described in detail in Oshun et al. (2021). The field campaigns occurred from June 2018 to September 2021 and focused on: 1) monitoring hydrologic inputs and outputs to calculate annual water balances; 2) determining spatiotemporal patterns in runoff through a novel campaign to measure discharge in nested subbasins ; 3) characterizing bofedal structure, installing monitoring wells, and employing borehole nuclear magnetic resonance (NMR) techniques to quantify the amount of water seasonally stored in bofedales seasonal water storage in bofedales. Our results show bofedales store large amounts of water seasonally, and the slow drainage of this water contributes to perennial streamflow in the humid puna.

2.0 Site Description and Methods

2.1 Site Description of the Upper Ramuschaka Watershed (URW)

The 2.12 km^2 URW sustains three perennial streams that form each of its three primary basins – the Western, (0.373 km^2), Central (0.873 km^2), and Eastern (0.797 km^2) (Figure 1). These basins form a confluence approximately 150 m upstream of the downstream terminus of the URW, at a concrete diversion weir used by the community of Zurite to divert surface water for irrigation.

The URW shows landscape features characteristic of the humid puna: bedrock outcrops, upland tussock grasslands, bofedales, and sparsely distributed xerophytic shrubs, primarily located in the lower elevation reaches of the catchment. The underlying bedrock of the URW is primarily the Eocene-age San Jeronimo Formation (Carlotto, 2010). The Central and Eastern basins are underlain by '*Capa Roja'* cliff -forming reddish-gray sandstone that is finely bedded to massive. The sandstone is interbedded with broad sections of tan to reddish gray to greenish gray finely bedded and extensively fractured weak mudstone, known as *lutita.* The *lutita* weathers to produce clay-rich soils. A sugary-white crystalline quartzite forms a steep bedrock-exposed ridge that divides two upper tributaries of the Central basin. The Western basin is predominantly underlain by the San Jeronimo Formation; however, limestone outcrops with extensive karst weathering are found in the headwaters of the Western basin. An Oligocene quartz monzodiorite intrusive underlies much of the lower western portion of the basin.

The headwaters of the URW are defined by cliff forming headwalls of quartzite or sandstone and more gently sloping *lutita*. Low gradient basins are found below these steep headwalls. Poorly distinguished moraines and hummocky landforms are found along the margins of low gradient valleys (Figure 2). The topography of the landscape combined with its southern aspect suggest recent glaciation, perhaps during the Holocene.

Steep uplands are predominantly covered in the perennial tussock grass, *Jarava ichu,* which we observed to be rooted to a depth of approximately 1.2 m. Hydrophytic plants are found in the seasonally saturated bofedales. Common species are *Distichia muscoide*s, *Oxychloe andina*, and *Plantago tabulosa*, but there is no *Sphagnum* moss, which is consistent with the *Distichia* peatlands presented in Maldanado Fonken (2014). The community of Zurite implemented efforts to stabilize hillslopes in the lower URW via afforestation with *Polylepis sp.* in 2018. Despite the afforestation campaign, most *Polylepis* shrubs remained small (1-2 meters tall with sparse branching) because of low growth rates through seasonal drought and a grassland fire in 2019.

2.2 Geospatial Characterization and Discharge Measurements

We combined land cover classification and topographic geospatial methods to characterize the URW and identify spatiotemporal relationships in URW water yield.

2.2.1 Land Cover Classification

We used *ENVI 5.5* (L3Harris Geospatial) to classify four land cover classes in the URW: ‘Bofedal’, ‘Upland’, ‘Outcrop’ and ‘Shrubland’. We performed supervised classification on 1-meter resolution Esri World Imagery of the URW with the support vector machine (SVM) algorithm following the ITT (2008) and L3Harris Geospatial (2019) methods. We quality controlled the resulting land cover classification vectors via ground truthing during field campaigns and with high-resolution (8.3 cm/pixel) orthoimagery produced from Unmanned Aerial Vehicle (UAV) surveys.

2.2.2 Topographic Data Collection and Processing

In June 2019, we flew a DJI Phantom 4 Pro UAV to collect photographic data of the URW with 80% coverage overlap at 200 feet above the ground surface. We deployed 26 Ground Control Points throughout the URW, surveyed with an Eos Real Time Kinematic (RTK) Global Positioning System (GPS) to ground truth photogrammetric elevation products (Supplementary Material S1). Reported mean horizontal error on surveyed GCPs was 0.097 m and mean vertical error was 0.113 m.

We used Agisoft Metashape Professional to post-process UAV surveys into 1-m/cell resolution Digital Elevation Map (DEM) and 8.3 cm/pixel resolution orthoimagery products using protocols from the United States Geologic Survey (2017) and Dietrich (2015). Watershed boundaries for the two stream gages, and targeted discharge points were delineated using the 1-m resolution DEM.

2.3 Hydrologic Monitoring

2.3.1 Annual Water Balance

We measured precipitation (P), evapotranspiration (*ET*), and runoff (*q*) to estimate interannual storage (ΔS) and construct annual water balances. Water balances are referenced to Site 3 (Figure 1). Uncertainty for each component of the annual water balance is reported in both mm and as a percentage of annual precipitation. In the following, we describe the methods for measuring or calculating *P, q,* and *ET.* Due to the incomplete data set for WY2019, which lacked upland soil and saprolite and groundwater measurements used to estimate ET, we focus our water balance analyses on WY2020 and WY2021.

2.3.2 Precipitation

Precipitation and air temperature were measured from June 2018 through March 2022 in the Central Basin, near Site 3 (4,171 m), using a HOBO Onset RG3 tipping bucket rain gage with a resolution of 0.2 mm. We also installed a RG3 rain gage in the in the town of Zurite at 3,411 m.

The start of the annual water year (September 1) corresponds with the end of the regionally dry austral winter and marks a gradual transition into the wet season. Here, we define the dry season as occurring when 15-day cumulative antecedent precipitation at the URW rain gage remained less than 10 mm. Conversely, the wet season was defined as the period when 15-day cumulative antecedent precipitation equaled or exceeded 10 mm.

There are no existing precipitation products (Aybar et al., 2020) with fine scale resolution to account for orographic effects between Zurite and the URW. To account for orographic effects, we extrapolated a per-meter difference in 15-day antecedent precipitation measured at our two tipping bucket rain gages installed in the URW and Zurite (Supplementary Material, S2). We note that the battery in the URW gage failed in September 2021, and we thus present precipitation data from Casa Zurite (3,411 m) for the WY2022 wet up.

2.3.3 Streamflow in the URW

In June 2018, we installed stream gages in the Central basin (Site 3) and directly above the diversion canal (Site 1) The area draining to Site 3 is 0.806 km^2 and the total area draining to Site 1 is 2.11 km^2. At each location, we connected a slotted PVC staff gage (with demarcations to 1/50th of a foot) to rebar stakes driven into the channel bed and installed one HOBO U20L-001 water level logger inside the pipe. A separate pressure transducer was installed in a streamside bush to account for barometric pressure. Measurements were taken at 15-minute intervals and logged in the sensor. Every 2- to 5-months data were manually downloaded and post-processed to account for any sensor drift or variability in reinstallation of the water level logger (Supplementary Material S2.3).

We measured stream discharge using the salt dilution technique (Hudson and Fraser, 2005) on 14 dates from June 2018 - August 2021 to develop rating curves relating stage height to discharge (Supplementary Material 2.3). At Site 3, we developed two rating curves separated before and after a high flow event in March 2019. At Site 1, the high flow event substantially changed the channel geometry. We present Site 1 data from April 2019 onward, using only one rating curve. We scale discharge by watershed area to present hydrographs of unit runoff (mm/day) for WY2019, WY2020, and WY2021. Runoff at Site 3 was used in water balances for WYs 2020 and 2021. Error in runoff estimates was calculated by the mean residual error from all discharge measurements used to develop each rating curve. We focus our analyses on Site 3 due to a better fit of the rating curve, lower error estimates, and because there were no changes in stream morphology over the length of the monitoring period.

2.3.4 Subsurface moisture dynamics and estimates of grassland evapotranspiration

We estimated ET fluxes from upland *J. Ichu* hillslopes by directly measuring changes in soil and saprolite moisture. In January 2019, we installed four Teros-12 volumetric water content (VWC) sensors (Meter Group Inc., 2018) horizontally in the upslope face of undisturbed soil and saprolite. Sensors were installed at depths of 20 cm and 60 cm (soil) and at 90 cm and 120 cm (saprolite). The sensors recorded VWC at 15-minute intervals. Data were manually downloaded every 2 to 5 months and post-processed to produce daily average VWC. We calculated seasonal dynamics of moisture storage (mm) over the profile by multiplying changes in VWC at each sensor by an assigned depth range (Supplementary Material S2.2).

To distinguish ET fluxes from drainage, we estimated field capacity (defined here as the VWC of a freely drained soil or saprolite) as the median VWC value between January 1 to April 15 (Supplementary Material S2). During this period, we assumed increases in VWC beyond field capacity resulted in vertical drainage below the depth of the sensors, and more importantly the rooting zone, leading to either increased moisture content in unsaturated weathered bedrock, or to groundwater recharge (e.g., Abdelnour et al., 2011). When soil moisture was greater than the field capacity estimate, we used a crop coefficient of 0.80 to convert potential evapotranspiration (PET) to actual evapotranspiration (AET) for the *J. ichu* grasses in the uplands. We assumed decreases in VWC below field capacity were due to plant-root uptake or evaporation (e.g., Abdelnour et al. 2011). We converted VWC to mm of storage by multiplying the VWC over the depth range of the sensor (Supplementary Material S2.2). ET was then calculated as the sum of moisture loss below field capacity across all layers of the rooting zone in mm/day. We extrapolated the ET in our measured profile to the area classified as ‘Upland’, which accounts for approximately 83% of the Site 3 subbasin and incorporated it in the annual water balances for WY2020, and WY2021. We estimated error in ET via the reported instrument error of +/- 3.00% for uncalibrated Teros-12 sensors in a mineral soil system (Meter Group, Inc, 2019). We acknowledge additional error may arise from extrapolating *J. Ichu* ET estimates to all areas classified as ‘Upland’.

2.3.5 Seasonal water dynamics and estimates of bofedal evapotranspiration

To estimate ET fluxes from seasonally saturated bofedales, we combined direct measurements of groundwater with a simple evaporative flux model. In June 2019, we drilled to 11m in Bofedal A and installed monitoring Well 102. Well 102 was cased using slotted 65 mm diameter PVC pipe with end caps. We installed a HOBO U20-001 30-ft water level logger to measure water table dynamics at 15-minute intervals. We manually measured the depth to the water table from the top of the well casing using a Solinist 101 (Georgetown, Ontario, Canada) water level meter when downloading water level data every 2 to 5 months.

ET fluxes from bofedales (which cover 11.6% of the URW) were estimated using a temperature-driven daily model in the Visualizing Ecosystems Land Management Assessment 2.0 (VELMA 2.0) graphical user interface (Abdelnour et al., 2011), which estimates PET by applying a modified version of Hamon (1963). When the water table was at the surface in Well 102, we assumed all bofedales across the URW were saturated and that AET from bofedales was equal to PET as water would evaporate off the surface of a lake. For time periods in which Well 102 was not saturated, we applied the AET estimates from our vertical VWC sensor array to the area classified as ‘Bofedal’ as a local approximation for AET. To account for error in PET estimates made from daily temperatures, we used the maximum error reported (+/- 30%) from Córdova et al., (2015), where temperature driven PET error was estimated in the Ecuadorian páramo - a similar, albeit wetter tropical alpine grass- and shrub-land system occurring in the Andes north of the puna.

2.4 Spatiotemporal Measurements of Discharge

To explore landscape controls on water yield, specifically the effects of bofedales, we measured discharge via salt dilution (Hudson and Fraser, 2005) at 19 nested locations on 14 dates between June 2019 and September 2021 (Figure 1). We designed our campaign to test the implicit assumption of constant unit runoff throughout the URW and to explore whether unit runoff might increase from subbasins with a greater proportion of bofedal cover. Discharge measurements were located within the Central (n = 9), Eastern (n = 8), and Western (n = 1) subbasins (Figure 1). All sites drained to Site1. The 'West' discharge point measured discharge from the Western subbasin - which we treated differently due to the widespread extent of limestone karst found exclusively in the Western basin headwaters. Subbasins topographic indices and bofedal extent are presented in Supplementary Material Table 1. Channel morphology ranged from relatively shallow-sloped reaches (local channel slope < 5%) that flowed through bofedal and wet alpine grassland settings to steep reaches (local channel slope >30%) with bedrock-confined flow. In most locations, the channel was incised into either bedrock, proglacial features, or bofedales.

2.5 Seasonal moisture dynamics in bofedales

2.5.1 Material and hydraulic properties of bofedales

To characterize material properties in bofedales we hand augered 33 boreholes across four bofedales in the Central and Eastern subbasins, referred to as bofedales ‘A’, ‘B’, ‘C’, and ‘D’ (Figure 1), in June 2019 (dry season) and January 2020 (wet season). Boreholes were augered with a 4-inch bucket auger along transects spanning from the upslope contributing hillslopes through the center of the bofedales. Sediments recovered from the boreholes were used to identify strata of peat, clay and underlying glaciofluvial deposits or weathered bedrock, henceforth referred to as the ‘mineral layer,’ along each transect. We extended the depth of a 3.2 m borehole in bofedal A to 11.1 m with the rotary drill to install Well 102.

In June 2019, we collected downhole NMR measurements in 11 boreholes in Bofedales A and B using a portable NMR Logging System (Dart, Vista Clara, Inc., Mukilteo, Washington, USA). NMR is a geophysical method used to determine the porosity or water content of sediments and to estimate pore-size distributions and hydraulic conductivity (e.g., Behroozmand et al., 2015). Measurements were collected downward from the ground surface elevation in 0.25 m increments. The volume of investigation of each measurement was a cylindrical shell of 0.23 m height, 1–2 mm in thickness at a radius of 6.5–7.6 cm from the central axis of the tool (Walsh et al., 2013). Additional details on instrument parameters and data processing can be found in Supplementary Material S3.

2.5.2 Estimates of bofedal dynamic water storage

To determine the seasonally dynamic water storage in bofedales, we first combined direct observations of sediment logs and NMR measurements in Bofedales A and B with continuous measurements of water table dynamics in Bofedal A, and water table observations in bofedales A-D. We then combined these data with direct observations of strata thicknesses to construct cross-sections and estimate seasonally dynamic water storage in bofedales A-D.

In each layer of the bofedal, we determined ‘drainable’ seasonally dynamic water storage, or the amount of stored water that may drain to streams, as the difference between total porosity (VWC at saturation) and the VWC at field capacity (e.g., Abdelnour et al., 2011). We derived porosity values in saturated peat, clay, and the underlying mineral layer from NMR logs in Bofedales A and B in June 2019. We estimated field capacity in peat to equal the VWC of unsaturated peat directly above the water table in June 2019. Clay and saprolite field capacities were determined from NMR measurements in unsaturated clay and saprolite at the margin of Bofedal B, in H5 and H6. We used the Inverse Distance Weighted (IDW) method in ArcGIS Desktop 10.1 software to interpolate the thicknesses of peat, clay and mineral layer strata and the water table depth between boreholes in bofedales A, B, C, and D in mid-dry season (June 2019) and mid-wet season (January 2020).

We determined seasonally dynamic water storage by estimating the difference between saturated water content and field capacity within the dynamic range of observed groundwater dynamics, which spanned from the soil surface to well into the clay layer in each bofedal cross section. Maximum water table depth was measured in Bofedal A (Well 102) and extrapolated to bofedal cross-sections B, C, and D. We divided the sum of cross-sectional dynamic storage by the length of the cross-section to calculate an average depth of dynamic storage for each bofedal. We present the depth of dynamic storage as a range derived from NMR saturated water content standard deviations in each layer. We then extrapolated average dynamic storage in the four bofedal cross-sections across the extent of all mapped bofedales in the URW to estimate the total volume of water seasonally stored in and released from bofedales.

3.0 Results

3.1 Annual Water Balances and Dry Season Runoff

Precipitation, subsurface moisture, groundwater, and runoff dynamics in the URW for WYs 2019 - 2021 followed seasonal cycles of an October to December wet-up, a sustained period of precipitation, high subsurface moisture and high runoff from December - April, and little to no precipitation and a prolonged recession in subsurface moisture and runoff from May - October (Figure 3). The shaded yellow bars indicate the dry seasons (defined by a 15-day cumulative precipitation below 10 mm) spanning from May or early-June until mid-October each year.

3.1.1 Precipitation

We measured 749 mm, 825 mm, and 738 mm of precipitation at the URW rain gage in WY2019, WY2020, and WY2021, respectively. Although the water year begins on September 1, 15-day cumulative precipitation did not rise above 10 mm until early- to mid-October in the three observed transitions from dry to wet season (Table 1). Wet season precipitation generally peaked in both frequency and intensity between December and April, however we also measured several stretches of lighter precipitation during each wet season. The average length of the three complete dry seasons (2019, 2020, and 2021) was 151 days, and the average dry season precipitation was 18.6 mm (Table 1).

Table 1: Each of the three dry season dates, number of days, and cumulative precipitation received in the URW over the monitoring period of WY2019-WY2021. The dry season is defined as the period when 15-day cumulative precipitation remained under 10 mm.

Dry Season	Dates	Number of days	Cumulative precipitation (mm)	Cumulative runoff at Site 3 (mm)
1	May 8th – Oct 4th, 2019	150	20.6	69.6
2	May 19th – Oct 18th, 2020	153	24.7	93.0
3	Jun 8th – Oct 1st, 2021	115	10.6	57.0

3.1.2 Subsurface moisture dynamics in the uplands

Soil and saprolite water storage increased with the first substantial precipitation events of the wet season, rose to a relatively stable wet season state, and declined steadily through the dry season. We identified field capacity in soil and saprolite to equal 310 and 214 mm of moisture, respectively. A similar amount of precipitation fell before field capacity was reached in each of the soil and the saprolite each year: 128 mm and 208 mm in WY 2020, 224 mm and 268 mm in WY 2021, and 152 and 192 mm in WY 22 for an average of 168 ± 50 and 223 ± 40 mm of precipitation to reach field capacity in the soil and saprolite, respectively. Successive storms caused peaks of increased water storage in the soil and saprolite which rapidly declined as water drained to recharge deeper layers in the unsaturated zone and groundwater. As precipitation tapered off at the end of the wet season, subsurface water storage declined below field capacity due to uptake by *J. Ichu*. The rate of recession was steeper in soil than in saprolite, however, rates declined in both media late in the dry season. By the end of the dry season, prior to the onset of precipitation, soil and saprolite water storage reached minimum values of 262 mm and 186 mm (Dry Season 1), 210 mm and 163 mm (Dry Season 2), and 222 and 174 (Dry Season 3), respectively. The lower water storage values in Dry Season 2 may have been the result of vigorous growth in recovering upland grasses following a mild grass fire that swept through much of the URW in July 2019, and likely led to the greater quantity of precipitation needed to reach soil and saprolite field capacities during the WY 2021 wet-up. Total plant available water for *J. ichu* is estimated as 151 mm: the difference between moisture at field capacity and minimum in the soil was 100 mm (310 - 210) and was 41 mm (214 - 163) in the saprolite.

3.1.3 Bofedal groundwater dynamics

We measured remarkably similar annual cycles of recharge, sustained wet season saturation, and groundwater recession in Well 102 (Bofedal A). The groundwater in Bofedal A responded immediately to the start of the wet season with a modest rise. Successive rain caused rapid rises in the groundwater table and complete saturation that roughly coincided with the timing of field capacity in the soil and saprolite in the hillslope. Bofedal A saturated on November 29th, 2019, after 173.8 mm of cumulative precipitation in WY 2020, on December 1st, 2020 after 181.5 mm of cumulative precipitation in WY2021 and on December 12th, 2021 after 192 mm of cumulative precipitation in WY 2022 (measured at the Casa Zurite rain gage at 3,411 m in WY 2022). The groundwater table remained at the surface through the wet seasons and well into the dry season. Bofedal A did not begin to desaturate until 55, 43, and 25 days into dry seasons 1, 2, and 3, respectively. Once Bofedal A desaturated, the water table decline was remarkably linear with rates of decline of 15.2, 13.4 and 13.3 mm/day in dry seasons 1, 2, and 3, respectively. The water table in Bofedal A reached a maximum depth of 1.77, 1.94, and 1.42 m below the ground surface in dry seasons 1, 2, and 3, respectively. In each complete dry season, the groundwater table fell over 1 m below the peat – clay transition, which was 0.6 m below the ground surface.

3.1.4 Runoff in the URW

In all water years, runoff at Site 3 did not rise substantially above baseflow conditions until after soil and saprolite water storage reached field capacity and Bofedal A saturated (Figure 3). In each water year, a similar amount of cumulative precipitation fell before runoff increased from baseflow to wet season conditions, which we define as greater than 1 mm/d, or 9.26 l/s at Site 3. In WYs 2019, 2020, 2021, and 2022; 292, 177, 206, and 156.4 mm of precipitation (WY 22 measured at the Casa Zurite gage at 3,411 m) fell before runoff exceeded 1 mm/d, respectively.

Throughout the wet season, runoff at Site 3 responded quickly to precipitation inputs (Figure 3). Peak flows reached 8.9 mm/d (83 l/s) in WY2019 and 10.7 mm/d (99 l/s) in WY 2020. In WY 2021, peak flows never exceeded 5 mm/d (47 l/s). The low peak flows in WY2021 were derived from the stage data itself, as both water years utilized the same rating curve. Accessibility constraints during the COVID-19 lockdowns resulted in less frequent measurements and limited our ability to fully resolve peak flow. Despite these limitations, medium and low flows in WY2021 plotted consistently on the rating curve (Supplementary Material S2.3).

Runoff declined steadily as the system entered the dry season. Across the three dry seasons, the rate and shape of runoff recessions was similar with baseflows of 0.13 mm/d (1.3 l/s), 0.25 mm/d (2.3 l/s), and 0.26 mm/d (2.5 l/s) in dry seasons 1, 2, and 3, respectively.

3.1.5 Annual Water Balances

We calculated similar annual water balances in WYs 2020 and 2021 (Table 2). Here, we report precipitation values adjusted for orographic effects by using the mean elevation value of the Site 3 subbasin (4,476 m.a.s.l.) (Supplementary Material 2.1). We report precipitation and runoff for WY2019, but do not calculate the water balance because subsurface moisture equipment was installed mid water year (January 2019). In WY 2019-2021, we estimated 797, 867, and 751 mm of annual precipitation. All annual precipitation values are within one standard deviation of the average gridded precipitation in Zurite (848 ± 156 mm) from 1981 - 2017 (Aybar et al., 2020).

Annual runoff followed precipitation trends, with 453 mm in WY 2019, 643 mm in WY 2020, and 439 mm in WY 2021. Runoff accounted for 57%, 74%, and 58% of precipitation in WYs 2019, 2020, and 2021, respectively. Differences in annual runoff across the three water years occurred primarily in the wet season. Dry season runoff, calculated from the beginning to the end of the dry season, was 69.6, 93.0 and 57.0 mm in dry seasons 1, 2, and 3, respectively (Table 1).

In WYs 2020 and 2021, the two years for which ET estimates could be made for an entire water year, ET accounted for 30% - 40% of the annual water balance. During WY2020, 80% of ET was estimated to be from uplands and 20% from bofedales. During WY2021, 78% of ET was estimated to be from uplands and 22% from bofedales.

The difference between annual inputs and outputs (ΔS in Table 2) combines interannual watershed storage, potential drainage below Site 3 (which we did not directly measure), and measurement error. In WY2020, ΔS was -63 mm, as outputs exceeded precipitation. In WY2021, ΔS was 27 mm, as precipitation exceeded outputs by 27 mm. Each estimate of ΔS falls within the combined errors of annual runoff and ET (Table 2).

Table 2: Annual water balances referenced to the Site 3 subbasin for WY2020 and WY 2021. Precipitation, runoff and ET (from January 2019 onward) are reported for WY 2019. Precipitation values used in each water balance represent the measured precipitation value at the URW rain gage adjusted for orographic effects on precipitation (See Supplementary Material S2 for methodology).

Site		**Precipitation**		**Runoff**		**Estimated ET**	**ΔS**
	Metric	***Wet season***	***Dry season***	***Wet season***	***Dry season (through WY only)***		
***A)* Site 3 WY2019**	**Total *(mm)***	775	17	393	59	122 ± 14	NA
		792 ± 8		452 ± 54			
	Percentage	100%		57% ± 12%		15% ± 11%	NA
***B)* Site 3 WY2020**	**Total *(mm)***	847	20	560	84	287 ± 22	-63
		867 ± 4		643 ± 84			
	Percentage	100%		74% ± 13%		33% ± 8%	-7
C) Site 3 WY2021	**Total *(mm)***	718	19	390	49	285 ± 23	27
		751 ± 1		439 ± 57			
	Percentage	100%		58% ± 13%		32% ± 8%	4

3.1.6 Temporal Phases of the Annual Water Balance

Figure 4 presents the cumulative fluxes of precipitation, ET, and runoff at Site 3 for WY 2020 and 2021 (data found in Supplementary Material S4). The seasonality of precipitation and hydrological response in the watershed divide the water year into three distinct phases: ‘fill-up’, ‘steady-state’ and ‘release’.

The fill-up phase began with the start of the WY, on September 1st, and continued until Well 102 (in Bofedal A) saturated. During the fill-up phase, precipitation exceeded the combined fluxes of runoff and ET by 4-5-fold as precipitation recharged depleted soil and saprolite moisture reservoirs and deeper (unmeasured) zones of unsaturated rock moisture and the water table. During the fill-up phase, groundwater in Well 102 began to rise, but cumulative runoff showed only modest increases.

The steady-state phase began with the saturation of Bofedal A. This coincided with a rise to field capacity in the shallow subsurface of the hillslope. Once Bofedal A saturated, the watershed entered a quasi steady-state in which successive precipitation caused rapid and larger stream runoff. During the steady-state phase, cumulative ET increased steadily due to increasing temperatures during the austral summer. Precipitation inputs roughly equaled the combined outputs of runoff and ET, with runoff accounting for 62 - 78%, and ET accounting for 17 - 26% of precipitation, respectively.

The release phase began when 15-day antecedent precipitation fell below 10 mm. This occurred on May 19th, 2020 in WY2020 and on June 8th, 2021 in WY2021. With a near absence of precipitation, the slope of cumulative runoff declined, but importantly continued to increase due to sustained streamflow through the dry season. Bofedal A did not desaturate until 43 and 25 days into the dry season. Baseflow throughout the release phase was sustained above 0.25

mm/day until the next water year's fill-up phase began. ET accounted for the greatest total moisture loss over the release period as upland grasses and hydrophytic vegetation sustained steady rates of transpiration, leading to depletion in shallow subsurface moisture storage that was recharged during the fill-up phase of the following water year.

3.1.7 Spatiotemporal patterns of runoff in the URW

Distributed streamflow measurements taken on 14 dates between June 2019 and August 2021 show a general positive correspondence across all seasons between the percent of each subbasin classified as bofedal and runoff (Figure 5). Data points are colored to show the corresponding flow percentile at Site 3, which corresponds to general flow conditions across all measurement points. The start of the dry season corresponded with the 58.4th flow percentile in WY2019, the 60.6th percentile in WY2020, and the 55.4th percentile in WY2021. The relationship between the percent of each subbasin covered in bofedal and runoff strengthened during the wet season.

Three stations show consistently higher runoff, falling along a trendline offset from other subbasins: the Western Basin, and Sites 1 and 2. We consider potential explanations for these discrepancies in the discussion.

3.2 Seasonally dynamic water storage in bofedales and their contributions to runoff

3.2.1 Bofedal Material Properties & Cross Section(s)

Bofedales are found in local topographic depressions and along watercourses, with greater extent in the large glacially carved basins of the upper URW (Figure 1). Borehole transects in Bofedales A, B, C, and D showed similar stratigraphy: a) hydrophytic vegetation b) highly porous dark peat c) highly plastic glaciofluvial clays and silts, and d) weathered clayey silty saprolite (Figure 6). The maximum depth of peat was 60 cm, 175 cm, 100 cm, and 50 cm in Bofedales A, B, C and D, respectively. In all bofedales, the depth of peat was the greatest near the centroid and tapered towards the surrounding hillslopes. A layer of highly plastic glaciofluvial clays and silts underlying the peat was 0- to 120 cm thick, with the clayey mineral layer extending several meters below the ground surface. In some boreholes, the distinction between fine clays and silts and clayey saprolite was marginal. In such instances, no glaciofluvial strata of fine clays and silts was reported. The cross-section of Bofedal B is shown in Figure 7, and all cross-sections are in the Supplementary Material S3. Hydrophytic plant roots generally extended beyond the depth of peat into underlying glaciofluvial sediments or mineral layers. The upslope contributing area to Bofedales A through D ranged from 4- to 12 times the area of each bofedal (Table 5, Supplementary Material, S3).

3.2.2 Bofedal Water Storage

We measured groundwater dynamics continuously in only Bofedal A (Well 102). However, in all bofedales we observed shallower water tables near the centroid and a deeper water table towards the hillslope in all seasons.

In June 2019, the mean depth to water table in bofedal A was 20 cm, and was 36 cm in Bofedal B. In January 2020, the average depth to the water table in bofedales A, B, C, and D was 14 cm, 11.6 cm, 9.5 cm, and 12.2 cm, respectively, with standing water across large portions of each bofedal. Material observations of bofedal strata and groundwater levels in Well 102 highlight the drainage of bofedal groundwater beyond the depth of peat and into glaciofluvial deposits and/or saprolite.

Downhole NMR data from 13 boreholes in bofedales A and B showed a decrease in total porosity, estimated field capacity, and hydraulic conductivity through the peat, clay, and underlying mineral layers. Table 3 presents mean porosity values for each layer. The porosity of each layer was strikingly consistent between the two bofedales as indicated by reported values and the small standard deviations. Mean porosity across all boreholes showed an extremely high porosity peat (0.88) underlain by lower porosity clay (0.51) and mineral layers (0.39). Field capacity estimates decrease with depth through the peat, clay and the underlying mineral layer. Drainable volumetric water content is largest in the peat (0.42) and decreases in the clay (0.21) and saprolite (0.19). Estimates of saturated hydraulic conductivity also decreased with depth from 14.3 m/d in the peat to 2.6 m/d in the clay, and 0.5 m/d in the saprolite.

Table 3: Calculated porosities and standard deviations for peat, clay, and the underlying mineral layer from saturated downhole NMR measurements during June 2019 surveys. Field capacity estimates were made from unsaturated NMR water content measurements in each layer at the margins of bofedales A and B in June 2019. Reported average porosity values per material layer were derived across the entire data set and thus may deviate from the average value of the reported porosities in bofedales A and B due to more measurements logged in bofedal B.

Subsurface stratum	**Peat (10 cm - 175 cm thickness)**	**Clay (0 cm - 120 cm thickness)**	**Underlying mineral layer (meters thickness)**
Bofedal A porosity	0.92 ± 0.12	0.46 ± 0.13	0.38 ± 0.046
Bofedal B porosity	0.86 ± 0.12	0.52 ± 0.13	0.39 ± 0.046

Mean NMR data set porosity	0.88 ± 0.12	0.51 ± 0.13	0.39 ± 0.046
Estimated VWC at field capacity	0.46	0.30	0.20
Drainable VWC: Porosity – Field Capacity	0.42	0.21	0.19
Mean saturated hydraulic conductivity (m/d)	14.3 ± 13.1	2.6 ± 6.2	0.5 ± 0.8

3.2.3 Seasonally dynamic water storage and runoff in the URW

Average dynamic storage within each of the four bofedales varied from 360 to 540 mm (Table 4). The broad range is a function of both the bofedal thickness – primarily the thickness of the peat, and to a lesser extent, the clay – and the total area of the bofedal. Larger bofedales had thicker peat deposits and thus greater average dynamic storage. Bofedal B, the largest bofedal in the URW, had the deepest mineral layer (measured to 3.2 m below the ground surface) and peat thickness of up to 175 cm in the center. Smaller bofedales such as A, C, and D, had thinner layers of peat (50 – 100 cm) above clay layers.

Across the URW, the 244,000 m^2 of bofedales dynamically store 105,000 ± 10,000 m^3 of water. This corresponds to 49 ± 5 mm of runoff at the scale of the 2.12 km^2 URW. Groundwater did not begin to decline in Well 102 until the release phase, which started 54, 44, and 24 days into dry seasons 1, 2, and 3, respectively. The dynamically stored water is thus not released from Bofedal A until well into the dry season. Conservatively, we can compare bofedal dynamic storage to *total* dry season runoff, which averaged 73.2 ± 18.2 mm at Site 3 and 114.9 ± 21.4

mm at Site 1. Water contributions from bofedales thus account for 67 ± 31% of dry season streamflow at Site 3, and 43 ± 22 % of dry season streamflow at Site 1.

Table 4: Size, upslope contributing area, and average dynamic storage in the four measured bofedales of the URW. Final row shows estimates of dynamic storage expressed as runoff, at the scale of the URW.

Site	**Area (m^2)**	**Contributing area (m^2)**	**Drainable dynamic storage (mm)**
Bofedal A	1,855	22,394	390±30
Bofedal B	84,932	428,391	540±60
Bofedal C	6,775	36,031	430±40
Bofedal D	27,373	112,923	360±30
Total in URW	244,000		49 ± 5

4.0 Discussion

Large and small Andean communities depend on water resources emanating from the humid puna; however, hydrologic data relating the physical structure of the humid puna, including bofedales, to water resources are limited. Here, we discuss our key findings in the context of our motivating questions by first comparing seasonal patterns in water yield from the URW with the few existing studies of water resources in high elevation and seasonally dry Andean landscapes. We highlight our discovery of higher unit runoff from subbasins with greater bofedal coverage and compare seasonally dynamic storage in bofedales with dry season runoff and downstream water needs. We briefly discuss the limitations of our analyses and then present a conceptual model highlighting the hydrological function of bofedales in regulating water resources and sustaining perennial streamflow in the humid puna.

4.1 Water Resources in the Humid Puna

Continuous runoff data spanning three complete water years show distinct wet-dry season dynamics. Runoff in the URW is controlled by precipitation inputs, reflecting the precipitation driven hydrograph of the 11,048 km^2 VUB (Drenkhan et al., 2015; Buytaert et al., 2017; Oshun et al., 2021). Runoff in the URW comprised 57%, 74%, and 58% of annual water balance inputs from WY2019 to WY2021, similar to runoff ratios reported in undisturbed Andean grasslands in the humid puna and the wetter páramos in the northern Andes (Ochoa-Tocachi et al., 2016; Mosquera et al., 2015). We compare the Flow Duration Curve (FDC) from the URW with FDCs of two undisturbed catchments in the humid puna (HUA1 and TIQ2, from Ochoa-Tocachi et al. 2016) and three undisturbed catchments in the wetter páramo of the Ecuadorian Andes (PAU1 from Ochoa-Tocachi et al., 2016 and ZEO M4 and M5 from Mosquera et al., 2015). All catchments are between 0.65 and 4.22 km^2, at elevations between 3700 and nearly 4800 m.a.s.l., have average slopes ranging from 9 to 21 %, and contain bofedales covering 3 to 18 % of the catchment area (Supplementary Material S5). Annual precipitation varies from a minimum of 803 mm in the URW to a maximum of 1358 mm at PAU1.

TIQ 1, in Bolivia, receives similar annual rainfall (835 mm) to the URW, yet yields only 0.29 of this rainfall as runoff. Although peak flows slightly exceed the URW, runoff at flow percentiles greater than approximately 5 are consistently smaller than the URW. The low runoff ratio and consistently lower runoff values may be attributable to few bofedales or interannual storage in cirque lakes and/or high rates of evaporation. HUA1, in the Cordillera Blanca, is one of the wettest catchments (1346 mm annual precipitation), yet the FDC is very steep, resulting in little baseflow. The ‘flashiness’ of HUA1 is likely the result of a pronounced dry season (similar to the URW), but also may be attributable to limited catchment wide storage due to very small bofedal coverage (estimated at 3-4% of the catchment) and steep headwalls of exposed bedrock.

Runoff in the three páramo catchments is consistently higher than in the URW. Peak runoff is 22-78 mm/d in the páramo, while peak runoff in the URW reaches only 10.7 mm/d. In the páramo, large annual rainfall and no distinct dry season (Balslev and Luteyn 1992; Luteyn 1999) result in smaller seasonal dynamics in catchment water storage (e.g., Buytaert et al., 2007), higher peak flows, and a relatively flat FDC. However, above a flow percentile of 10%, the general shape of the FDCs of the páramo catchments is similar to the FDC of the URW. The relatively high sustained runoff and the ‘flatness’ of the FDC in the URW is remarkable because, unlike the páramo, the humid puna landscape receives little to no rain for approximately 5 months. The hydrograph in the URW shows a gradual recession, with dry season runoff accounting for 13 - 16% of annual water yield. The flatness of the FDC suggests dry season runoff is sustained by seasonally dynamic water storage at the scale of the URW (e.g., Searcy, 1959; Buytaert et al., 2007; Yadav et al., 2007; Ochoa-Tocachi et al., 2016). Dry season runoff from the puna is extremely important for downstream population centers, such as Zurite and Cusco (Drenkhan et al., 2015, Ochoa-Tocachi et al., 2016; Wunderlich, 2021; Oshun et al., 2021; SEDACUSO, 2021), and will only be more critical as the puna biome expands (Tovar et al., 2013).

4.2 Bofedales and Water Yield in the URW

We found higher runoff in subbasins with greater bofedal extent. A similar study exploring connections between landscape characteristics and runoff also found a positive correlation between peak runoff and wetland coverage in the páramo of Ecuador (Mosquera et al., 2015). Others have related large proportions of wetland cover to limited catchment-wide storage capacity, shedding of excess water (e.g., Rodhe, 1987), and high peak flows (Pearce, 1990; Burt, 1995; Quinton et al., 2003; Bullock and Acreman, 2003) dominated by 'event-water' (e.g., Laudon et al., 2007). However, the spatiotemporal patterns in runoff in the URW differ from these studies in two primary ways. First, we found no relationships between bofedal coverage or mean runoff and the size of the subbasin. Second, we found that in addition to larger peak runoff, *baseflow* was also consistently larger in subbasins with greater bofedal coverage. This final observation is consistent with measurements of greater baseflow in boreal catchments with thicker sedimentary deposits and wetlands (e.g., Karlsen et al., 2016; Floriancic et al., 2019).

Runoff was anomalously high at three sites in the lower part or the URW: Site 1, Site 2, and the Western subbasin. Mean slope throughout these three subbasins was between 23 - 25°, slightly higher than in other subbasins. Between Site 3 and Site 2, the morphology of the valley changes from a broad, U-shaped valley to a narrow, V-shaped valley with a steep, bedrock-confined channel. Changes in morphology from glaciated valleys to deeply incised stream morphology result in higher sustained runoff (Prancevic and Kirchner, 2019; Gillespie & Clark, 2011; Whiting & Godsey, 2016). Large runoff in the Western subbasin is likely associated with mapped limestone karst in the headwaters, which is known to store and release large volumes of water (e.g., Villacorta et al., 2016; Somers and McKenzie, 2020). Although our study did not focus on characterizing limestone karst in the Western basin, electrical conductivity was consistently 50 to 80% greater at the West site than elsewhere in the URW, consistent with higher rates of chemical dissolution from the more soluble limestone. Site 1 integrated large runoff values from Site 2 and the Western subbasin and maintained baseflow above 0.39 mm/d (9.5 l/s). We interpret these high runoff values in the lower URW to be driven by morphologic and lithologic controls in addition to dynamic storage in bofedales.

4.3 Dynamic storage in bofedales, quantifying contributions to streamflow

Bofedales A-D integrate upslope contributing areas 4 - 12 times their size (Table 5). Groundwater in Well 102 showed a rapid response leading to saturation of Bofedal A coinciding with the timing of field capacity in the hillslope (Figure 3). These two observations suggest that bofedales fill in response to rapid delivery of groundwater from large upslope contributing areas, consistent with recent studies in southern Perú and Chile (Cooper et al., 2019; Valois et al., 2020; Valois et al, 2021).

NMR measurements show the drainable porosity of peat to be 0.42, or about 47% of total porosity. This value is consistent with estimates of peat water yield ranging from 10 - 80%, depending on the degree of organic decomposition (Radforth and Brawner, 1977; Letts et al., 2000). By combining our drainable porosity estimates in peat, clay and saprolite with water table dynamics in Bofedal A, we estimate bofedales A- D seasonally store an average of 360 - 540 mm of water.

We are aware of only two studies quantifying water storage capacity in bofedales, which were both conducted in streamside bofedales in a narrow canyon of the Estero Derecho watershed in Chile. The bofedales are approximately 2 hectares in area (smaller than Bofedal D) and composed of an approximately 0.3 m layer of peat and underlying fluvial deposits and colluvium to an estimated depth of 10m (Valois et al., 2020; Valois et al., 2021). Here, the authors calculated total porosity to a depth of 10 m to estimate a total water storage of between 1,000 and 3,400 mm. Without measurements of drainable porosity and water table dynamics, it is difficult to estimate how much water these bofedales would contribute to streamflow; however, if we assume the water table drops 2 m below the surface and apply our estimate of drainable rather than total porosity to 0.3 m of peat (0.42), and 1.7 m of underlying deposits (0.21), we estimate dynamic storage to be 483 mm. This estimate is consistent with bofedales A-D and highlights the large contributions of bofedales to dry season streamflow, as well as the importance of quantifying hydraulic properties of the different material layers of bofedales and monitoring water table dynamics.

The 244,000 m^2 of bofedales in the URW dynamically store 105,000 ± 10,000 m^3 of water. Importantly, this dynamically stored water accounts for up to 98% of dry season runoff, sustaining surface flow when irrigation demands in Zurite are the greatest. From the time the bofedales begin to drain (early July) to the start of the wet season (early to mid-October), irrigation demand in Zurite is approximately 730 mm (Wunderlich, 2021, Oshun et al., 2021). *Chacras*, or family-owned agricultural plots are typically 0.25 to 1 hectare (Oshun et al., 2021). Water draining from bofedales in the URW thus meets the dry season irrigation demand of 13.0 – 15.7 hectares, equivalent to between 13 and 63 familial plots.

4.4 Limitations and potential error in bofedal dynamic storage estimates

We were unable to explicitly account for two possible errors in our estimates of seasonally dynamic water storage in bofedales. First, despite our sampling of material properties across four bofedales, we could not capture all spatial heterogeneity, hydraulic parameters, and water table fluctuations in the entire URW. Whereas our measurements of porosity were well constrained, we did not fully characterize relationships between bofedal size, location, and the thickness of peat, clay and underlying layers. The second potential source of error derived from our application of groundwater dynamics in Bofedal A to bofedales B-D. Extreme topography prevented us from transporting a drill rig to bofedales B-D, and we were thus unable to install a monitoring well. We note that saturation of Well 102 coincided with the timing of field capacity in the rooting zone of hillslope grasses, immediately preceded sustained high runoff values throughout the URW, and that Well 102 did not begin to drain until well into the dry season. Therefore, although we did not monitor groundwater in all bofedales, the temporal correspondence between hydrologic events throughout the watershed and our field observations of mid wet season saturation in Bofedales A-D, support our interpretation that bofedales across the URW have similar temporal patterns to Bofedal A.

4.5 Conceptual Model of Bofedal Hydrology

Bofedales form an important hydrologic interface between groundwater draining humid puna uplands and streamflow. We interpret bofedales as ‘waystations’ that collect groundwater contributions and regulate the release of this water to streams (Figure 8). Although our study is the first to quantify the hydrology of bofedales in the context of water resources in the humid puna, previous studies have shown water flowing through wetlands to have longer mean transit times (e.g., Lyon et al., 2010; Lane et al., 2019) and argued the presence of wetlands increases catchment wide water storage (Lane et al., 2019). We find bofedales increase catchment wide water storage and sustain baseflow through three key characteristics. First, the topographic location of bofedales, a product of the glacially carved landscape and terrestrialized basin, results in groundwater contributions from hillslopes 4 -12 times their size. Secondly, thick layers of high porosity (and high water yield) peat form a tremendously large reservoir in which to seasonally store water. Thirdly, the combined effects of a low gradient water table and low conductivity underlying layers of clay and saprolite, result in the slow release of water from bofedales to streams.

In Figure 8, we detail the hydrologic role of bofedales in the context of the observed temporal dynamics (three-phases) in streamflow. The onset of precipitation at the beginning of the water year marks the start of the Fill-up phase. Subsurface soil and saprolite moisture on the hillslope have been depleted well below field capacity due to grassland ET, and the groundwater table in bofedales is 1-2 m below the ground surface. Precipitation first recharges the rooting zone of grasses on the hillslope. A small response is seen in bofedal groundwater, most likely due to direct precipitation. In our three years of monitoring, field capacity in the soil and saprolite was reached after an average of 168 and 223 mm of cumulative precipitation, respectively. As field capacity is reached, groundwater in Bofedal A rises rapidly and Bofedal A saturates. Saturation of Bofedal A occurred after an average of 187 mm of cumulative precipitation. Once bofedales saturate, the system enters the Steady-State phase. At this point, the URW reaches its storage capacity, and runoff rapidly increases as the catchment sheds successive precipitation. We note that significant water is likely fluxing through or across bofedales as saturation overland flow during the Steady-State phase, but their saturated state prevents additional water storage. During this phase, the sum of cumulative runoff and ET is approximately equal to cumulative precipitation. Once cumulative 15 day-precipitation falls below 10 mm, the system enters the Release phase. With little to no precipitation, moisture within the rooting zone falls below field capacity due to evapotranspiration. Groundwater within hillslopes continues to drain through bofedales to streams and bofedales remain saturated for an average of 41 days into the dry season. Through the remainder of the dry season, the water table in bofedales declines linearly at an average rate of 14 mm/day as bofedales yield their dynamically stored water to sustain streamflow. Additional moisture depletion in the peat below field capacity occurs due to evaporation and transpiration of hydrophytic plants.

5.0 Conclusion

The URW, a 2.12 km^2 humid puna catchment draining to the agrarian village of Zurite, yields 57 - 74 % of the 803 mm of average annual rainfall to runoff. Despite a dry season lasting up to 5 months, the FDC of the URW is relatively flat due to large seasonally dynamic water storage at the catchment scale. Spatiotemporal discharge measurements throughout the URW identified greater runoff emanating from subbasins with greater bofedal coverage across all seasons. Three key characteristics of bofedales make bofedales vital shallow water aquifers with large seasonally dynamic water storage. First, bofedales are found in topographic depressions that collect water from upslope areas 4-12 times their size. Second, high porosity peat up to 1.5 m thick seasonally stores tremendous volumes of water. Third, a low water table gradient in gently sloping bofedales and the low conductivity of underlying layers of clay and glaciofluvial deposits/weathered bedrock result in the slow drainage of stored water. We estimate $105{,}000 \pm 10{,}000$ m^3 of water is dynamically stored in bofedales, equivalent to 49 ± 5 mm of runoff at the scale of the URW. Bofedales, which drain in the dry season, account for 20 -98% of dry season flow in the URW, sufficient to meet the irrigation demands of 13 - 15 hectares. We conclude that bofedales regulate flow to sustain perennial streams in the humid puna and are thus vital infrastructures to local and regional water security.

Wyeth Wunderlich: Conceptualization, Methodology, Formal Analysis, Investigation, Data curation, Writing – original draft and review & editing. **Margaret Lang**: Methodology, Investigation, Resources, Writing – review & editing, Supervision, Funding acquisition. **Kristina Keating:** Methodology**,** Investigation**,** Analysis, Writing – review & editing, Supervision, Funding acquisition. **Wilner Bandera Perez**: Investigation. **Jasper Oshun**: Conceptualization, Investigation, Resources, Writing – original draft and review & editing, Supervision, Project administration, Funding acquisition.

Acknowledgements

This work would not have been possible without the support of the community of Zurite. We thank Tomás Ruiz López for his leadership in the community of Zuirte and Sr. Ruiz López, Gladis Quispe Giorgina Calanchi, and Marilin Ruiz Quispe for their hospitality. Uriel Ccopa Villena provided logistical support. René Pumayalli Saloma provided rotary drilling and connected us with local geology students. Many students contributed to this research. Laurel Smith designed and executed the drone flights in 2019. Alyssa Virgil and Hannah Gidanian surveyed in most of the geospatial data. Nolan Marshall augered many of the boreholes, logged material layers and analyzed data. Nicholas Hawthorne selected sites and installed the stream gages at Sites 1 and 3. Wilner Bandera was assisted in the field by Vidal Barrientos. Olivia Helprin, Jared Walbert, and Edward Davis mapped the geology. Other students who contributed to this work are: Peter Duin, Jillian Freiheit, Malia Gonzalez, Yojana Miraya, Hunter Murray, Johannes Ruiz Quispe, Joel Ruiz Quispe, Emily Santos, and Logan Schmidt. Thank you to Daniel Anaya for saving our subsurface moisture equipment from a grassland fire. Thank you to Bob and Susan McPherson for donating the RTK GPS and drone. Wyeth Wunderlich was supported by the Bud Burke Scholarship and by Lost Coast Rotaract in Eureka. This project was funded by Geoscientists Without Borders (GWB), of the Society for Exploration Geophysicists, [grant number 2017080009] and the National Science Foundation IRES program [grant number 2107395], with supplementary funding provided by a Rutgers Global Environmental Change Grant. None of the funding agencies were involved in the collection, analysis and interpretation of data, writing the manuscript, or the decision to submit the article for publication.

References

Abdelnour, A., Stieglitz, M., Feifei, P., McKane, R. (2011). Catchment hydrological responses to forest harvest amount and spatial pattern. Water Resources Research, 27:9, DOI: https://doi.org/10.1029/2010WR010165.

Aybar, C., Fernández, C., Huerta, A., Lavado, W., Vega, F., Felipe-Obando, O. (2020). Construction of a high-resolution gridded rainfall dataset for Perú from 1981 to the present day, Hydrological Sciences Journal, 65:5, 770-785, DOI: 10.1080/02626667.2019.1649411.

Balslev H, Luteyn JL (eds) (1992) Páramo: an Andean ecosystem under human influence. Academic Press, London

Baraer M, McKenzie JM, Mark BG, Bury J and Knox S (2009). Characterizing contributions of glacier melt and groundwater during the dry season in a poorly gauged catchment of the Cordillera Blanca (Perú). Adv. Geosci., 22, 41–49.

Bradley, R. S., Vuille, M., Diaz, H., and Vergara, W., (2006). Threats to water supplies in the tropical Andes. Science, 312: 1755–1756.

Bryant FC and Farfan RD (1984) Dry season forage selection by Alpaca [Lama pacos] in Southern Peru. *Journal of Range Management* 37: 330–333.

Bullock, A., Acreman, M. (2003). The role of wetlands in the hydrological cycle. Hydrol. Earth Syst. Sci. 7, 358–389.

Burt, T.P. (1995). The role of wetlands in runoff generation from headwater catchments. In: Hughes, M.R., Heathwaite, A.L. (Eds.), Hydrology and Hydrogeochemistry of British Wetlands. Wiley, Chichester, U.K.

Buytaert W, Iñiguez V, De Bièvre B. (2007). The effects of afforestation and cultivation on water yield in the Andean páramo. Forest Ecology and Management 251(1–2): 22–30. DOI:10.1016/j.foreco.2007.06.035

Buytaert, W., Célleri, R., & Timbe, L. (2009). Predicting climate change impacts on water resources in the tropical Andes: Effects of GCM uncertainty. Geophysical Research Letters, 36(7).

Buytaert, W. Beven, K. (2011). Models as multiple working hypotheses: hydrological simulation of tropical alpine wetlands. Hydrological Processes. 24, 1784-1799(2011). DOI: 10.1002/hyp.7936

Buytaert, W., Moulds, S., Acosta, L., De Bievre, B., Olmos, C., Villacis, M., ... & Verbist, K. M. (2017). Glacial melt content of water use in the tropical Andes. Environmental Research Letters, 12(11), 114014.

Carlotto, V., Concha, R., Cárdenas, J., Garcia, B., Villafuerte, C. (2010) Geoloía y Geodinåamica en la Quebrada Qenqo: Aluviones que Afectaron Zurite-Cusco. Informe Tecnico. INGEMMET, UNSAAC.

Célleri R., Buytaerte W., Bievre B., Tobon C., Crespo, P., Molina, J. Feyen, J. (2010). Understanding the hydrology of tropical Andean ecosystems through an Andean Network of Basins. IAHSAISH Publication 336: 209–212.

Cooper, D. J., Wolf, E., Colson, C., Vering, W., Granda, A., and Meyer, M. (2010). Alpine peatlands of the Andes, Cajamarca, Peru. Arctic, Antarctic, and Alpine Research, 42: 19–33.

Cooper, D. J., Sueltenfuss, J., Oyague, E., Yager, K., Slayback, D., Caballero, E. M. C., Mark, B. G. (2019). Drivers of peatland water table dynamics in the Central Andes, Bolivia and Perú. Hydrological Processes, 33(13), 1913–1925. https://doi.org/10.1002/hyp.13446.

Córdova M, Carrillo-Rojas G, Crespo P, Wilcox B, Célleri R. (2015). Evaluation of the Penman-Monteith (FAO 56PM) method for calculating reference evapotranspiration using limited data. Mountain Research and Development 35(3): 230–239. DOI:10.1659/MRDJOURNAL- D-14-0024.1

Dietrich, J. (2015). Agisoft Photoscan Crash Course. Advanced Geographic Research, online blog, accessed 10/4/2018.

Drenkhan, F., Guardamino, L., Huggel, C., and Frey, H. (2018). Current and Future Glacier and lake Assessment in the Deglaciating Vilcanota-Urubamba basin, Peruvian Andes. Glob. Planet. Change 169, 105–118. doi:10.1016/j.gloplacha.2018.07.005

Drenkhan, F. Huggel, C. Guardamino, L. Haeberli, W. (2019). Managing risks and future options from new lakes in the deglaciating Andes of Peru: The example of the Vilcanota-Urubamba basin. Science of the Total Environment 665 (2019) 465–483.

Drenkhan, F., Carey, M., Huggel, C., Seidel, J., Ore, M.T. (2015). The changing water cycle: climatic and socio-economic drivers of water-related changes in the Andes of Peru.WIREs Water, 2 (2015), pp. 715-733.

Engel, Z., Skrzypek, G., Chuman, T., Šefrna, L., & Mihaljevič, M. (2014). Climate in the Western Cordillera of the Central Andes over the last 4300 years. *Quaternary Science Reviews*, *99*, 60-77.

EPS SEDA CUSCO S.A. (2019). Memoria Anual 2019. Wanchaq, Cusco. (In Spanish). Accessed online January 2021. https://www.sedacusco.com/transparencia/memoria/2019.pdf

Fernandez-Palomino, C. A., Hattermann, F. F., Krysanova, V., Vega-Jácome, F., & Bronstert, A. (2021). Towards a more consistent eco-hydrological modelling through multi-objective calibration: a case study in the Andean Vilcanota River basin, Peru. Hydrological Sciences Journal, 66(1), 59-74.

Floriancic, M. G., Fischer, B. M., Molnar, P., Kirchner, J. W., & Van Meerveld, I. H. (2019). Spatial variability in specific discharge and streamwater chemistry during low flows: Results from snapshot sampling campaigns in eleven Swiss catchments. Hydrological Processes, 33(22), 2847-2866.

Flores-Ochoa J. 1977. Pastores de Puna: Uywamichiq Punarunakuna. Lima, Peru: Instituto de Estudios Peruanos.

Flores, E., Tácuna, R., & Calvo, V. (2014). Marco conceptual y metodológico para estimar el estado de salud de los bofedales. Perú. Ministerio del Ambiente.

Garreaud, R. D. (2009). The Andes climate and weather. Advances in Geosciences. 22, 3-11.

Garreaud, R., Vuille, M., Compagnucci, R., and Marengo, J. (2009) Present-day South American climate. Paleogeography, Paleoclimatology, Paleoecology. doi:10.1016.

Gillespie, A. R., & Clark, D. H. (2011). Glaciations of the sierra Nevada, California, USA. In *Developments in Quaternary Sciences* (Vol. 15, pp. 447-462). Elsevier.

Gordon, R. P., Lautz, L. K., McKenzie, J. M., Mark, B. G., Chávez, D., & Baraer, M. (2015). Sources and pathways of stream generation in tropical proglacial valleys of the Cordillera Blanca, Peru. Journal of Hydrology, 522, 628-644.

Hribljan, J.A., Cooper, D.J., Sueltenfuss, J., Wolf, E.C., Heckman, K.A., Lilleskov, E.A. & Chimner, R.A. (2015). Carbon storage and long-term rate of accumulation in high-altitude Andean peatlands of Bolivia. Mires and Peat, 15(12), 1–14.

Hudson, R., & Fraser, J. (2005). The mass balance (or dry injection) method. Streamline Watershed Management Bulletin, 9(1), 6-12.

Josse, C., Cuesta, F., Navarro, G., Barrena, V., Cabrera, E., Chacón-Moreno, E., Ferreira, W., Peralvo, M., Saito, J. & Tovar, A. (2009) Ecosistemas de los Andes del Norte y Centro. Bolivia, Colombia, Ecuador, Perú y Venezuela. (Ecosystems of Northern and Central Andes. Bolivia, Colombia, Ecuador, Peru and Venezuela). Documento Técnico, Programa Regional ECOBONA-Intercooperation, CONDESAN-Proyecto Páramo Andino, Programa BioAndes, Secretaría General de la Comunidad Andina, Lima, 96 pp. (in Spanish).

Karlsen, R. H., Grabs, T., Bishop, K., Buffam, I., Laudon, H., & Seibert, J. (2016). Landscape controls on spatiotemporal discharge variability in a boreal catchment. Water Resources Research, 52(8), 6541-6556.

Laudon, H., Sjoblom, V., Buffam, I., Seibert, J., Morth, M., (2007). The role of catchment scale and landscape characteristics for runoff generation of boreal streams. J. Hydrol. 344, 198–209.

Letts, M. G., Roulet, N. T., Comer, N. T., Skarupa, M. R., & Verseghy, D. L. (2000). Parametrization of peatland hydraulic properties for the Canadian Land Surface Scheme. Atmosphere-Ocean, 38(1), 141-160.

Lindsay, J. B. The Whitebox Geospatial Analysis Tools Project and Open-Acess GIS. Proceedings of the GIS Research UK 22nd Annual Conference, The University of Glasgow, 2014.

Luteyn JL (1999) Páramos: A Checklist of Plant Diversity, Geographical Distribution, and Botanical Literature. New York Botanical Garden Press, Bronx

Lyon, S. W., Laudon, H., Seibert, J., Mörth, M., Tetzlaff, D., & Bishop, K. H. (2010). Controls on snowmelt water mean transit times in northern boreal catchments. *Hydrological Processes*, *24*(12), 1672-1684.

Maldanado Fonken, M. (2014). An introduction to the bofedales of the Peruvian High Andes. Mires and Peat Volume 15(Article 4): 1-13.

Ministry of the Environment. (2019). Guía de evaluación del estado del Ecosistema de bofedal. Ministry of the Environment.

Mosquera, G. Lazo, P. Celleri, r. Wilcox, B. Crespo, P. 2015. Runoff from tropical alpine grasslands increases with areal extent of wetlands. Catena, 125(2015)120-128.

Municipalidad Dsitrital de Zurite. (2017). Plan de Desarrollo Concertado del Distrito de Zurite al 2017 (Spanish). Accessed online: https://www.scribd.com/document/436252392/PLAN-DE-DESARROLLO-CONCERTADO-DEL-DISTRITO-DE-ZURITE-AL-2017.

Ochoa-Tocachi, B., et al. (2016), Impacts of land use on the hydrological response of tropical Andean catchments, Hydrol. Processes, doi:10.1002/hyp.10980.

Ochoa Tocachi, B. F. et al. (2018). High-resolution hydrometeorological data from a network of headwater catchments in the tropical Andes. Sci. Data 5, 180080 (2018).

Oshun, J., Keating, K., Lang, M., & Miraya Oscco, Y. (2021). Interdisciplinary Water Development in the Peruvian Highlands: The Case for Including the Coproduction of Knowledge in Socio-Hydrology. Hydrology, 8(3), 112.

Oyague Passuni, Eduardo & Cooper, David. (2020). Peatlands of the Central Andes Puna, South America. 37. 255-260.

Oyague, E., Cooper, D. J., & Ingol, E. (2022). Effects of land use on the hydrologic regime, vegetation, and hydraulic conductivity of peatlands in the central Peruvian Andes. *Journal of Hydrology*, *609*, 127687.

Patty L, Halloy SR, Hiltbrunner E et al. (2010) Biomass alloca- tion in herbaceous plants under grazing impact in the high semi-arid Andes. *Flora-Morphology, Distribution, Func- tional Ecology of Plants* 205: 695–703.

Pearce, A.J. (1990). Streamflow generation processes—an austral view. Water Resour. Res. 26, 3037–3047.

Polk, M. H. Young, K. R. Cano, A. Leon, B. (2019). Vegetation of Andean wetlands (bofedales) in Huascarán National Park, Peru. Mires and Peat, Volume 24 (2019), Article 01, 1–26. DOI: 10.19189/MaP.2018.SNPG.387.

Prancevic, J. P., & Kirchner, J. W. (2019). Topographic controls on the extension and retraction of flowing streams. Geophysical Research Letters, 46(4), 2084-2092.

Quinton, W.L., Hayashi, M., Pietroniro, A. (2003). Connectivity and storage functions of channel fens and flat bogs in northern basins. Hydrol. Process. 17, 3665–3684

Radforth, N. W., & Brawner, C. O. (1977). Muskeg and the northern environment in Canada. In Muskeg Research Conference 1973: Edmonton, Alta.). University of Toronto Press.

Reiner RJ and Bryant F (1986) Botanical composition and nutri- tional quality of alpaca diets in two Andean rangeland com- munities. *Journal of Range Management* 39: 424–427.

Rodhe, A. (1987), The origin of streamwater traced by oxygen-18, PhD thesis, UNGI Rep. Ser. A 41,Uppsala Univ., Uppsala, Sweden.

Salvador, F., Monerris, J., and Rochefort, L. (2014). Peatlands of the Peruvian Puna ecoregion: types, characteristics and disturbance. Mires and Peat, 15 (article 03): 1–17.

Searcy, J. K. (1959). Flow-duration curves (No. 1542). US Government Printing Office.

Somers, L. D., McKenzie, J. M., Mark, B. G., Lagos, P., Ng, G. H. C., Wickert, A. D., ... & Silva, Y. (2019). Groundwater buffers decreasing glacier melt in an Andean watershed—but not forever. *Geophysical Research Letters*, *46*(22), 13016-13026.

Somers, L. D., & McKenzie, J. M. (2020). A review of groundwater in high mountain environments. Wiley Interdisciplinary Reviews: Water, 7(6), e1475.

Squeo, F. A., Warner, B., Aravena, R., and Espinoza, D. (2006). Bofedales: high altitude peatland of the central Andes. Revista Chilena de Historia Natural, 79: 245–255.

Tovar, C., Arnillas, C. A., Cuesta, F., & Buytaert, W. (2013). Diverging responses of tropical Andean biomes under future climate conditions. PloS one, 8(5), e63634.

United States Geologic Survey. (2017). Unmanned Aircraft Systems Data Post-Processing Structure-from-Motion Photogrammetry. National Unmanned Aircraft Systems (UAS) Project Office.

Valois, R., Schaffer, N., Figueroa, R., Maldonado, A., Yáñez, E., Hevia, A., & MacDonell, S. (2020). Characterizing the water storage capacity and hydrological role of mountain peatlands in the arid andes of North-Central Chile. Water, 12(4), 1071.

Valois, R., Araya Vargas, J., MacDonell, S., Guzmán Pinones, C., Fernandoy, F., Yánez Carrizo, G., & Maldonado, A. (2021). Improving the underground structural characterization and hydrological functioning of an Andean peatland using geoelectrics and water stable isotopes in semi-arid Chile. Environmental Earth Sciences, 80(1), 1-14.

Villacorta, S.; Rodríguez, C., Peña, F.; Jaimes, F. y Luza, C. (2016). Caracterización geodinámica y dendrocronología como base para la evaluación de procesos geohidrológicos en la cuenca del río Mariño, Abancay (Perú). Serie Correlación Geológica, 32 (1-2), 25-42.

Vining, B. R., Steinman, B. A., Abbott, M. B., & Woods, A. (2019). Paleoclimatic and archaeological evidence from Lake Suches for highland Andean refugia during the arid middle-Holocene. *The Holocene, 29*(2), 328-344.

Vuille, M., Francou, B., Wagnon, P., Juen, I., Kaser, G., Mark, B., and Bradley, R. (2008). Climate change and tropical Andean glaciers: past, present, and future. Earth Science Reviews, 89: 79–96.

Whiting, J. A., & Godsey, S. E. (2016). Discontinuous headwater stream networks with stable flowheads, Salmon River basin, Idaho. *Hydrological Processes*, *30*(13), 2305-2316.

White-Nockleby, C., Prieto, M., Yager, K., & Meneses, R. I. (2021). Understanding bofedales as cultural landscapes in the central Andes. *Wetlands*, *41*(8), 1-14.

Yadav M, Wagener T, Gupta H. (2007). Regionalization of constraints on expected watershed response behavior for improved predictions in ungauged basins. Advances in Water Resources 30: 1756–1774.DOI:10.1016/j.advwatres.2007.01.005

Yager, K., Prieto, M., & Meneses, R. I. (2021). Reframing Pastoral Practices of Bofedal Management to Increase the Resilience of Andean Water Towers. Mountain Research and Development, 41(4), A1-A9.

Figures and Captions

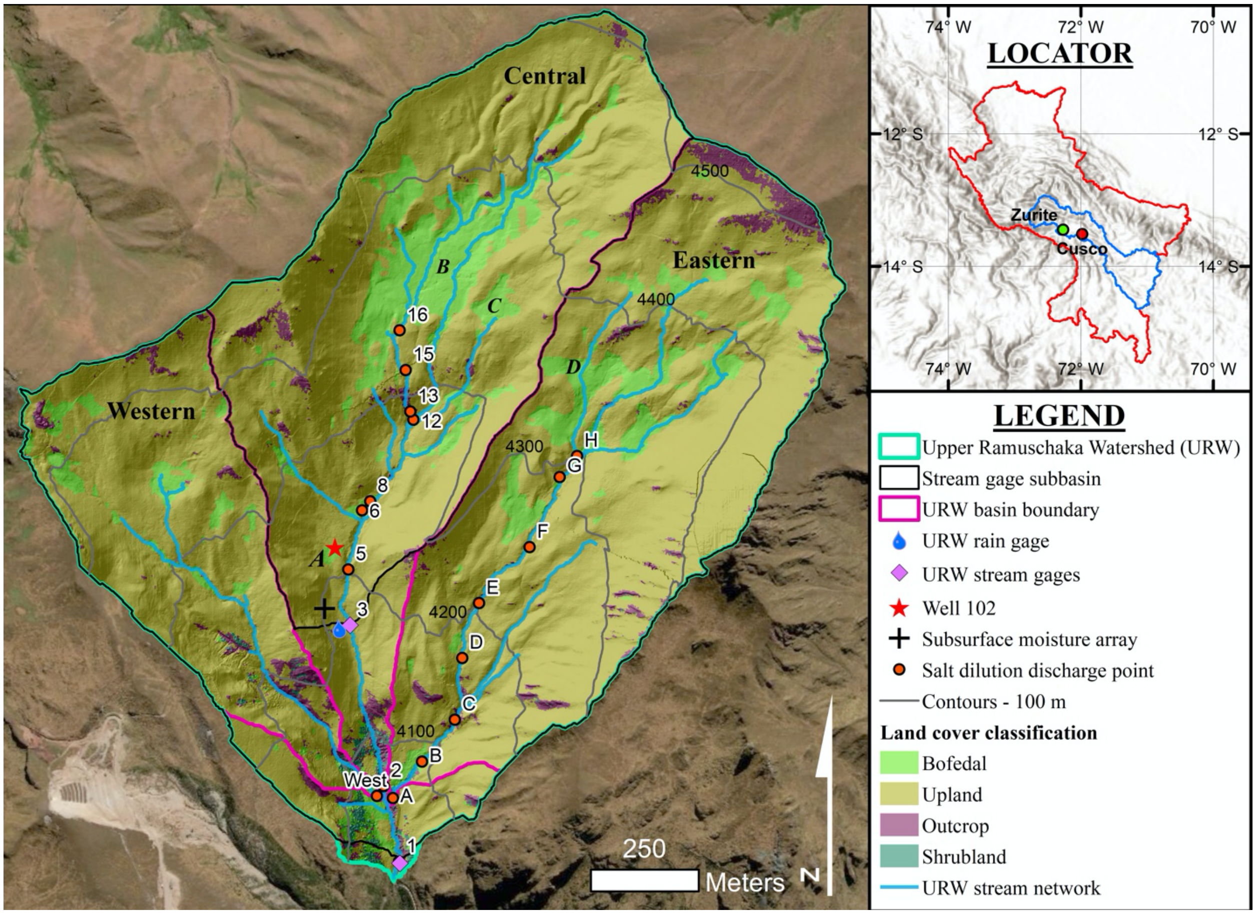

Figure 1: The URW (mean elevation: 4,332 m) is a 2.12 km^2 headwater humid puna catchment above the agrarian district of Zurite. The URW is within the Vilcanota Urubamba Basin in the department of Cusco (blue and red outlines, respectively in locator map). The URW has four primary land cover types: Bofedal, Upland, Outcrop, and Shrubland. Each of the three basins – the Western, Central and Eastern – yield perennial streamflow that forms a confluence just upstream from a concrete diversion weir at base of the URW. Locations of hydrologic monitoring instruments used to measure precipitation, subsurface moisture and groundwater dynamics, and stream discharge are shown, along with the subbasin boundaries draining to Site 3 (0.806 km^2). Locations of spatially distributed discharge measurements are shown with numbers in the Central Basin and letters in the Eastern Basin.

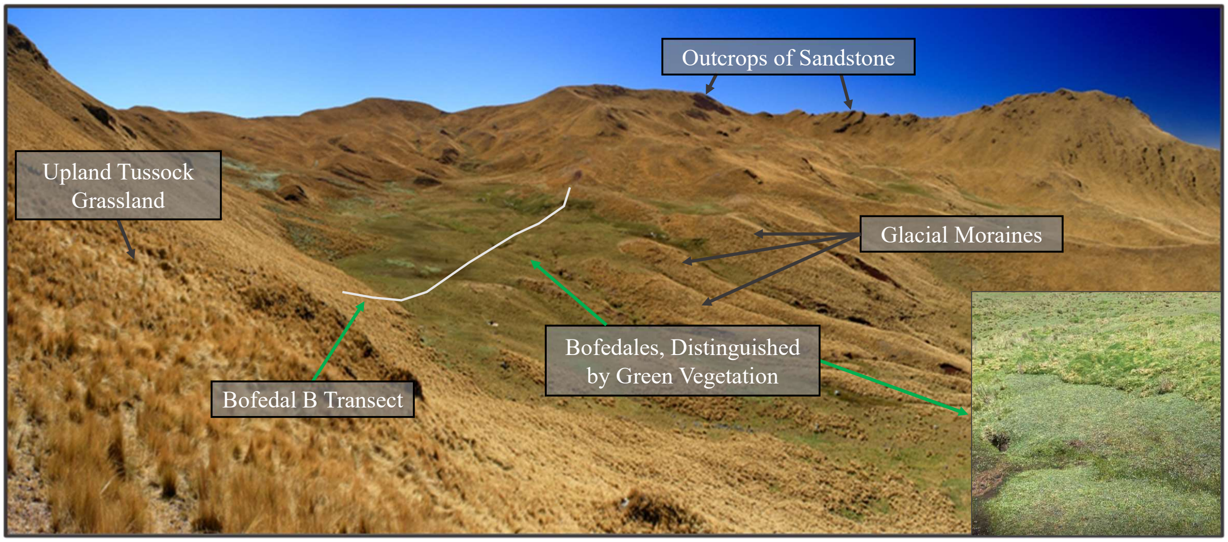

Figure 2: View overlooking the largest bofedal in the URW, Bofedal B. Direction of view is to the Northeast. The location of the Bofedal B survey transect is drawn in for reference. The ridgeline above the bofedal is the upper boundary of the Central Basin. The ridgeline from the center of the photograph to the right defines the boundary of the Eastern Basin. The photograph shows three of the four defined landcovers: Bofedal, Upland covered in *J. ichu,* and Outcrop. Shrubland is found only in the lower reaches of the catchment.

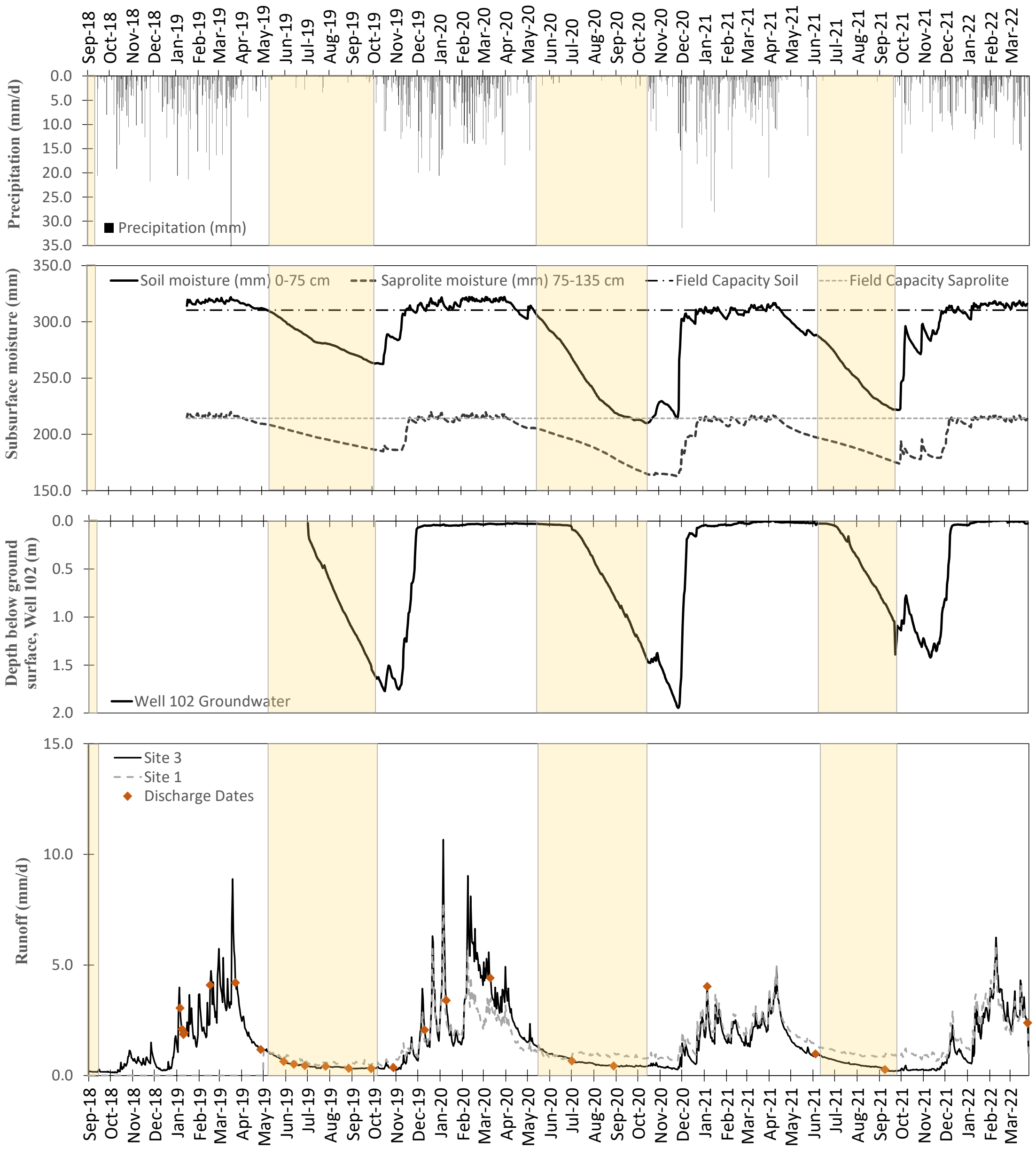

Figure 3: Time series plots of hydrological data over the monitoring period (September 2018 – March 2022). Upper panel shows daily precipitation at the URW rain gage. Second panel shows seasonal dynamics in moisture storage in soil and in saprolite. Dashed line indicates estimated field capacity in the soil and in the saprolite. Third panel shows groundwater dynamic at Well 102, which is in the center of Bofedal A. Bottom panel shows runoff in mm/day at Sites 1 and 3. The yellow highlighted periods denote the dry season, defined as the period when 15-day cumulative precipitation remained under 10 mm.

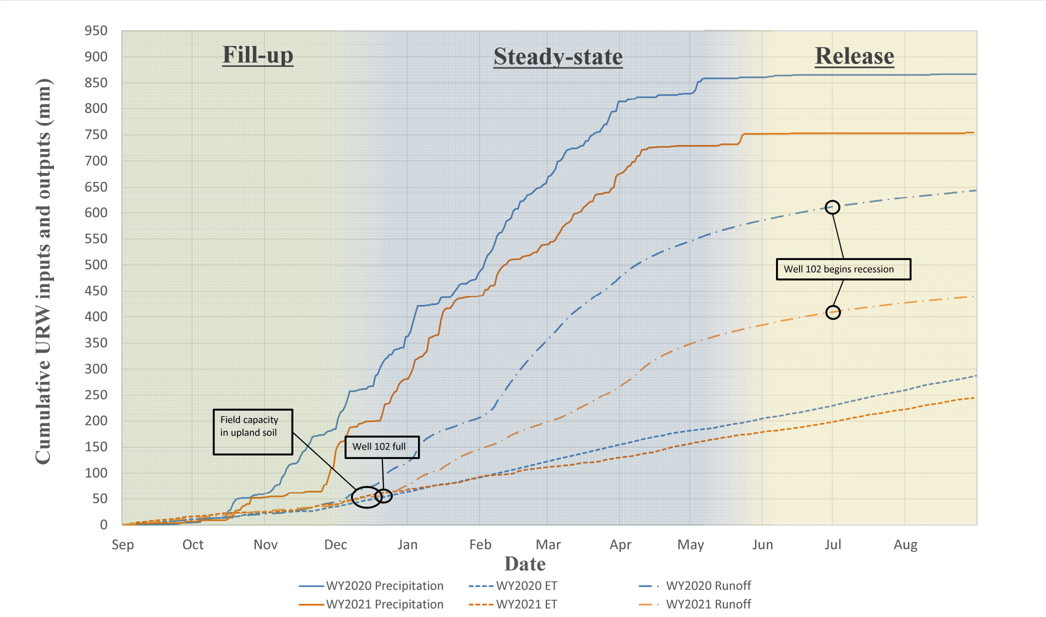

Figure 4: Cumulative fluxes of water through the URW for WYs 2020 and 2021. The seasonality of precipitation and resulting patterns in runoff and ET define three phases: fill-up, steady state, and release. The fill-up phase is defined by recharge of the unsaturated zone, and responses in Bofedal A. In the steady state phase, precipitation and the combined fluxes of runoff and ET are approximately equal. In the release phase, little to know precipitation falls, as water drains hillslopes, and importantly, bofedales. In the release phase, cumulative runoff tapers due to the dry season recession in streamflow.

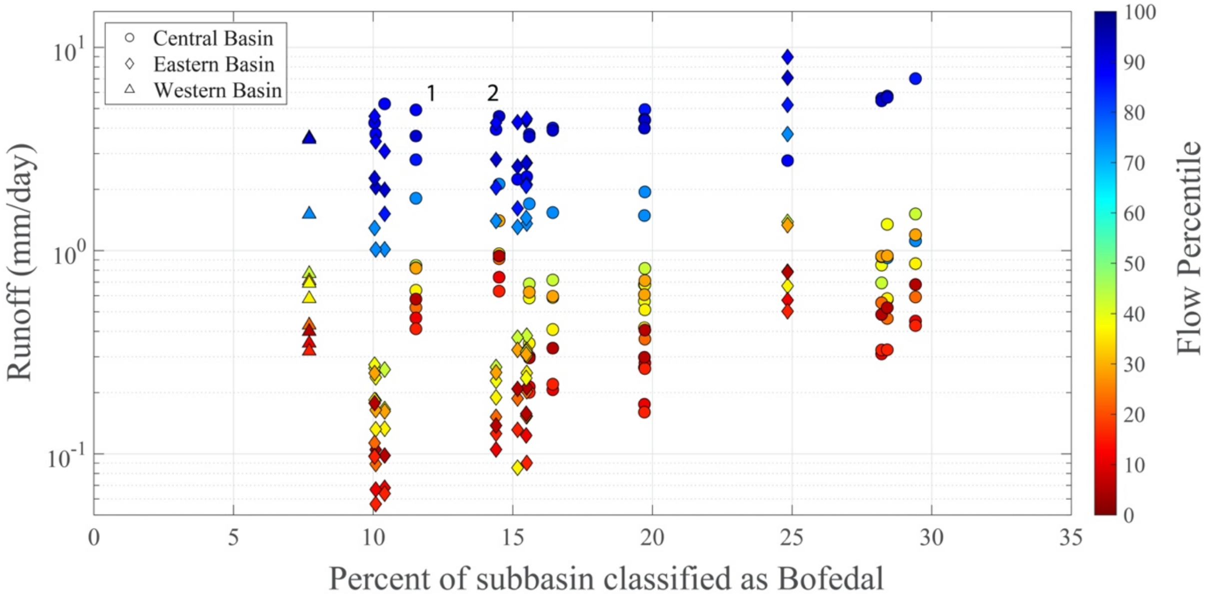

Figure 5: Scatterplot of the percent of each subbasin classified as bofedal (x-axis, linear) plotted against runoff (y-axis, log scale) for subbasins in the URW. The color-bar represents flow percentile at Site 3 over the course of water years 2019-2021. We measured discharge from the Western subbasin but treated it separately due to the abundance of karst weathered limestone in the upper Western subbasin not present in either the Central or Eastern subbasins. Best fit relationships show a linear trend for the wettest conditions ($q = 0.2135*(\%_{\text{bofedal}}) - 0.0338$, $r^2 = 0.62$), and a power law fit for the driest conditions ($q = 0.0076*(\%_{\text{bofedal}})^{1.29}$, $r2 = 0.40$).

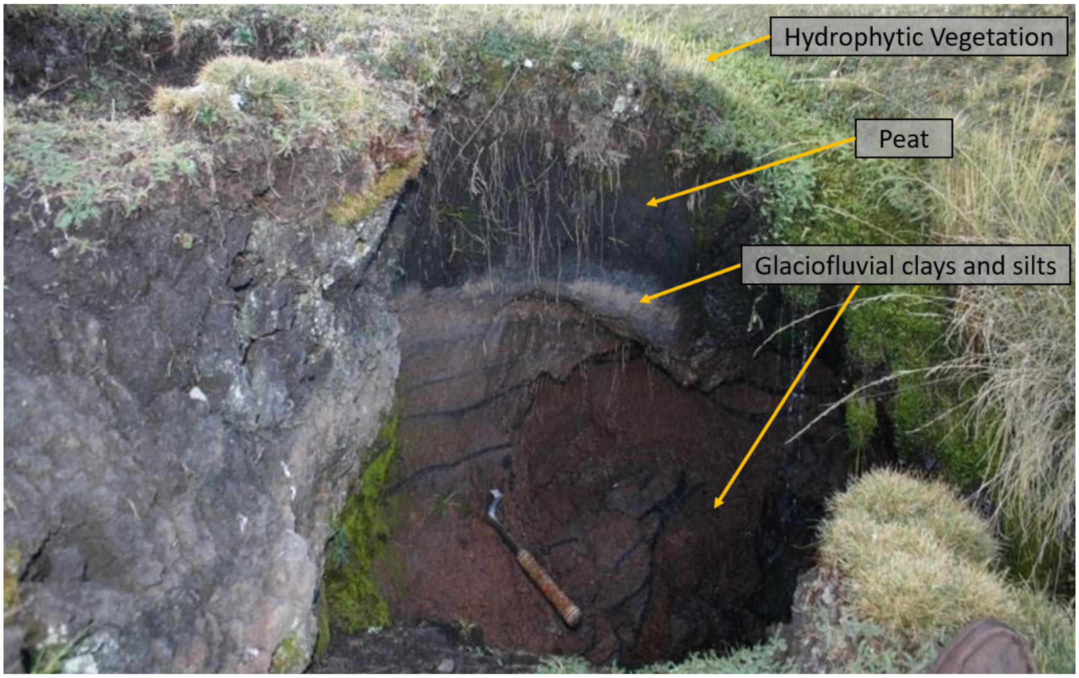

Figure 6: Bofedal stratigraphy showing hydrophytic vegetation, peat, and glaciofluvial clays. Not shown is the underlying layer of weathered bedrock. Photo taken in Bofedal B with a rock hammer for scale. At the time of this picture (mid dry season), water was flowing out along the boundary between the peak and glaciofluvial clay.

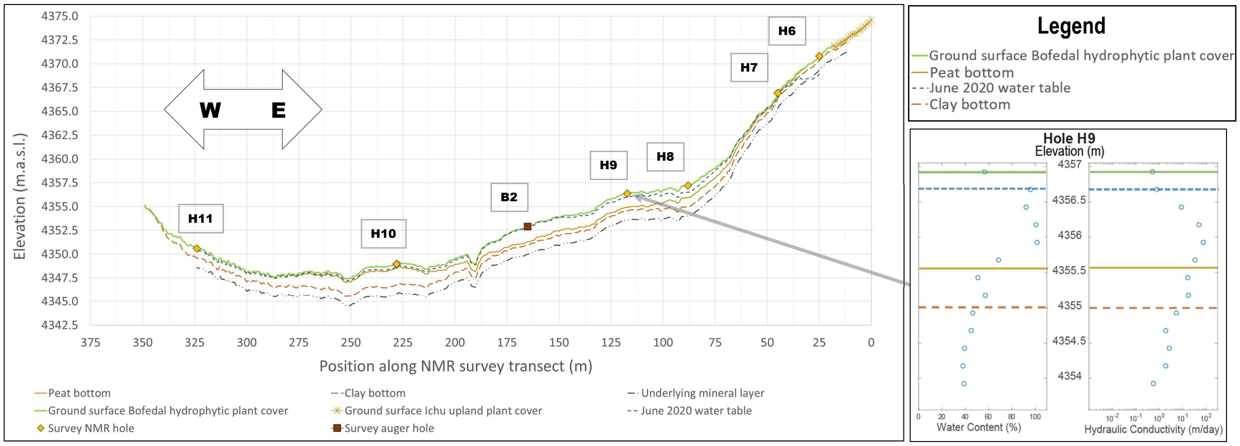

Figure 7: East-west cross-section of Bofedal B. Boreholes were augered in June 2019 and January 2020. The y-axis is vertically exaggerated 5 times. Profiles are generated via a combination of borehole logs and downhole nuclear magnetic resonance (NMR) calculations of water content. We extracted the ground surface elevation of points along the transect from a 1-meter DEM that we produced from a photogrammetry drone survey, and extracted layer depth and porosity values using an inverse distance weighted (IDW) spatial interpolation approach in ArcMap 10.6 Desktop. Dynamic water storage was estimated for the cross-sectional area below the depth of the January 2020 water table to a depth of 1.94 m below the ground surface, the greatest bofedal depth to water table observed in the URW.

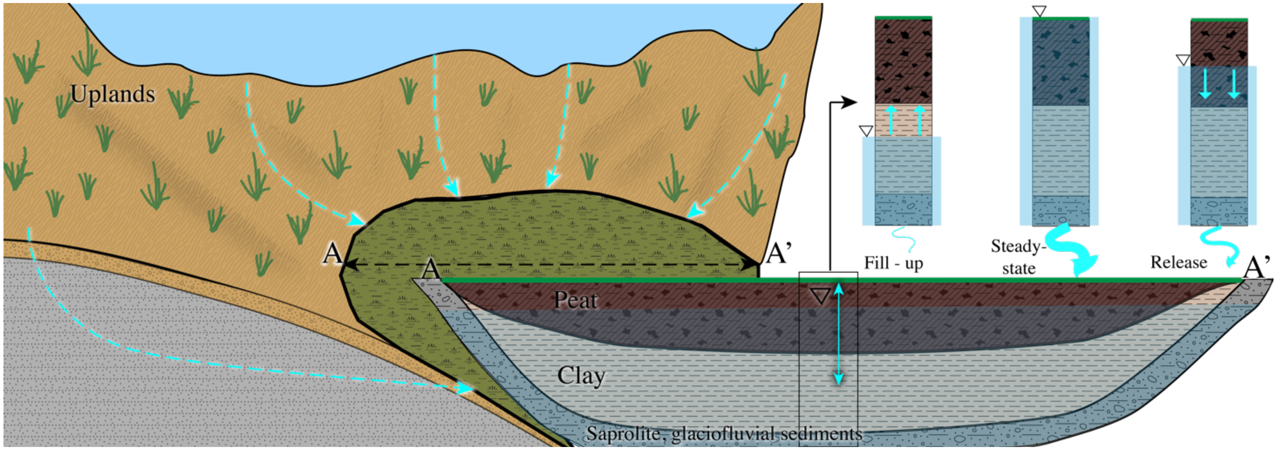

Figure 8. Conceptual model showing the hydrologic regulation of bofedales. A large contributing upland area (4 - 12 times the size of the bofedal) drains to bofedal. Groundwater contributions (shown with dashed blue lines) fill layers of clay and high porosity peat during the fill-up phase. Runoff in streams is small. Once the bofedal saturates, catchment wide storage capacity is filled, and successive storms generate rapid and large runoff responses. In the release phase, bofedales drain slowly, releasing water that sustains baseflow.